Oxygen Transport Ceramic Membranes

Quarterly Report

January 2004 – March 2004

Principal Authors:

Prof. S. Bandopadhyay

Dr. N. Nagabhushana

Issued: May 2004

DOE Award # DE-FC26-99FT40054

School of Mineral Engineering,
University of Alaska Fairbanks
Fairbanks, AK 99775

Contributing sub contractors:

1. **X.-D Zhou, Q. Cai, J. Yang, W. B. Yelon, W. J. James and H. U. Anderson,** Materials Research Center, University of Missouri-Rolla, Rolla, MO 65401
2. **Prof. Alan Jacobson and Prof. C.A. Mims;** University of Houston/University of Toronto

DISCLAIMER

ABSTRACT

The present quarterly report describes some of the investigations on the structural properties of dense OTM bars provided by Praxair and studies on newer composition of Ti doped LSF.

In this report, in situ neutron diffraction was used to characterize the chemical and structural properties of $La_{0.2}Sr_{0.8}Fe_{0.55}Ti_{0.45}O_{3-\delta}$ (here after as L2SF55T) specimen, which was subject to measurements of neutron diffraction from room temperature to 900ºC. It was found that space group of R3c yielded a better refinement than a cubic structure of Pm3m. Oxygen occupancy was nearly 3 in the region from room temperature to 700ºC, above which the occupancy decreased due to oxygen loss.

Dense OTM bars provided by Praxair were loaded to fracture at varying stress rates. Studies were done at room temperature in air and at 1000ºC in a specified environment to evaluate slow crack growth behavior. The X-Ray data and fracture mechanisms points to non-equilibrium decomposition of the LSFCO OTM membrane. The non-equilibrium conditions could probably be due to the nature of the applied stress field (stressing rates) and leads to transition in crystal structures and increased kinetics of decomposition. The formations of a Brownmillerite or Sr2Fe2O5 type structures, which are orthorhombic are attributed to the ordering of oxygen vacancies. The cubic to orthorhombic transitions leads to 2.6% increase in strains and thus residual stresses generated could influence the fracture behavior of the OTM membrane.

Continued investigations on the thermodynamic properties (stability and phase-separation behavior) and total conductivity of prototype membrane materials were carried out. The data are needed together with the kinetic information to develop a complete model for the membrane transport. Previously characterization, stoichiometry and conductivity measurements for samples of $La_{0.2}Sr_{0.8}Fe_{0.55}Ti_{0.45}O_{3-\delta}$ were reported. In this report, measurements of the chemical and thermal expansion as a function of temperature and p_{O2} are described.

TABLE OF CONTENTS

INTRODUCTION		1
EXECUTIVE SUMMARY		3
Task 1	Preparation and Characterization of Dense Ceramic oxygen Permeable Membranes	4
Task 2	Determine material mechanical properties under conditions of high temperature and reactive atmosphere	10
Task 3	Measurement of Surface Activation/Reaction rates in Ion Transport Membranes using Isotope Tracer and Transient Kinetic Techniques	18
CONCLUSIONS		25
REFERENCES		26
BIBLIOGRAPHY		27
LISTS OF ACRONYMS AND ABBREVIATIONS		28

LIST OF GRAPHICAL MATERIALS

Fig. 1. a^* as function of measuring temperature for *in situ* neutron diffraction, where a' was refined fro Pm3m and other two were refined from R3c.

Fig. 2. Oxygen occupancy and unit cell volume as a function of measuring temperature, in which data were refined from space group of Pm3m.

Fig. 3. Oxygen occupancy and unit cell volume as a function of measuring temperature, in which data were refined from space group of R3c.

Fig. 4. Lattice parameter (a and c) as a function of measuring temperature, in which data were refined from space group of R3c.

Fig. 5 XRD plots of the OTM samples in a) as received, b) exposed to Air at 1000ºC; c) exposed to N_2/Air at 1000ºC and fractured at varying stress rates in N_2/Air at 1000ºC

Fig. 6 XRD of the major peaks (2Theta = 32 and 77) plots of the OTM samples indicating a perceptible shift and decomposition of the single peaks.

Fig. 7: Surface flaw as fracture origin

Fig. 8: Intergranular fracture in OTM bars

Fig. 9a: Intergranular fracture of grains along in OTM with presence of fine precipitates

Fig. 9b: Trans/Intergranular fracture and formation of fine precipitates

Fig.10: Interaction of microstructure with presence secondary cracks. Increased formation of precipitates is observed

Fig.11: Transgranular fracture and presence of two types of precipitates

Fig.12: Slow transgranular crack growth with increased formation of two types of precipitates

Fig.13: Fast Transgranular fracture at the edge. The so called compressive curl consistently leads to transgranular fracture.

Fig. 14 Dilatometry data for $La_{0.2}Sr_{0.8}Fe_{0.55}Ti_{0.45}O_{3-\delta}$ (a) dL vs. time and (b) dL vs. temperature. The dotted line in a indicates the temperature profile.

Fig. 15(a) Chemical expansion data for $La_{0.2}Sr_{0.8}Fe_{0.55}Ti_{0.45}O_{3-\delta}$ - dL vs. time for the switch at 1000 °C.

Fig. 15b Chemical expansion data for $La_{0.2}Sr_{0.8}Fe_{0.55}Ti_{0.45}O_{3-\delta}$ - relative dL vs. time for the switch at 1000 °C.

Fig. 16(a) Expansion of $La_{0.2}Sr_{0.8}Fe_{0.55}Ti_{0.45}O_{3-\delta}$ in air and argon, the difference between the two lines is the chemical expansion on changing from $pO_2 = 0.21$ atm to 2×10^{-4} atm; (b) the change in chemical expansion with temperature.

INTRODUCTION

Conversion of natural gas to liquid fuels and chemicals is a major goal for the Nation as it enters the 21st Century. Technically robust and economically viable processes are needed to capture the value of the vast reserves of natural gas on Alaska's North Slope, and wean the Nation from dependence on foreign petroleum sources. Technologies that are emerging to fulfill this need are all based syngas as an intermediate. Syngas (a mixture of hydrogen and carbon monoxide) is a fundamental building block from which chemicals and fuels can be derived. Lower cost syngas translates directly into more cost-competitive fuels and chemicals.

The currently practiced commercial technology for making syngas is either steam methane reforming (SMR) or a two-step process involving cryogenic oxygen separation followed by natural gas partial oxidation (POX). These high-energy, capital-intensive processes do not always produce syngas at a cost that makes its derivatives competitive with current petroleum-based fuels and chemicals.

In the mid 80's BP invented a radically new technology concept that will have a major economic and energy efficiency impact on the conversion of natural gas to liquid fuels, hydrogen, and chemicals.[1] This technology, called Electropox, integrates oxygen separation with the oxidation and steam reforming of natural gas into a single process to produce syngas with an economic advantage of 30 to 50 percent over conventional technologies.[2]

The Electropox process uses novel and proprietary solid metal oxide ceramic oxygen transport membranes [OTMs], which selectively conduct both oxide ions and electrons through their lattice structure at elevated temperatures.[3] Under the influence of an oxygen partial pressure gradient, oxygen ions move through the dense, nonporous membrane lattice at high rates with

---

[1]Mazanec, T. J.; Cable, T. L.; Frye, J. G., Jr.; US 4,793,904, 27 Dec **1988**, assigned to The Standard Oil Company (now BP America), Mazanec, T. J.; Cable, T. L.; US 4,802,958, 7 Feb **1989**, assigned to the Standard Oil Co. (now BP America), Cable, T. L.; Mazanec, T. J.; Frye, J. G., Jr.; European Patent Application 0399833, 24 May **1990**, published 28 November **1990.**

[2]Bredesen, R.; Sogge, J.; "A Technical and Economic Assessment of Membrane Reactors for Hydrogen and Syngas Production" presented at Seminar on the Ecol. Applic. of Innovative Membrane Technology in the Chemical Industry", Cetraro, Calabria, Italy, 1-4 May **1996**.

[3]Mazanec, T.J., *Interface*, **1996**; Mazanec, T.J., *Solid State Ionics*, 70/71, **1994** 11-19; "Electropox: BP's Novel Oxidation Technology", T.J. Mazanec, pp 212-225, in "The Role of Oxygen in Improving Chemical Processes", M. Fetizon and W.J. Thomas, eds, Royal Society of Chemistry, London, **1993**; "Electropox: BP's Novel Oxidation Technology", T.J. Mazanec, pp 85-96, in "The Activation of Dioxygen and Homogeneous Catalytic Oxidation", D.H.R. Barton, A. E. Martell, D.T. Sawyer, eds, Plenum Press, New York, **1993**; "Electrocatalytic Cells for Chemical Reaction", T.J. Mazanec, T.L. Cable, J.G. Frye, Jr.; Prep Petrol Div ACS, San Fran, **1992** *37*, 135-146; T.J. Mazanec, T.L. Cable, J.G. Frye, Jr.; *Solid State Ionics*, **1992**, 53-56, 111-118.

100 percent selectivity. Transported oxygen reacts with natural gas on the fuel side of the ceramic membrane in the presence of a catalyst to produce syngas.

In 1997 BP entered into an OTM Alliance with Praxair, Amoco, Statoil and Sasol to advance the Electropox technology in an industrially sponsored development program. These five companies have been joined by Phillips Petroleum and now are carrying out a multi-year $40+ million program to develop and commercialize the technology. The program targets materials, manufacturing and engineering development issues and culminates in the operation of semi-works and demonstration scale prototype units.

The Electropox process represents a truly revolutionary technology for conversion of natural gas to synthesis gas not only because it combines the three separate unit operations of oxygen separation, methane oxidation and methane steam reforming into a single step, but also because it employs a chemically active ceramic material in a fundamentally new way. On numerous fronts the commercialization of Electropox demands solutions to problems that have never before been accomplished. Basic problems in materials and catalysts, membrane fabrication, model development, and reactor engineering all need solutions to achieve commercial success.

Six important issues have been selected as needing understanding on a fundamental level at which the applied Alliance program cannot achieve the breadth and depth of understanding needed for rapid advancement. These issues include:

1. Oxygen diffusion kinetics (University of Houston);
2. Phase stability and stress development (University of Missouri - Rolla);
3. Mechanical property evaluation in thermal and chemical stress fields (University of Alaska Fairbanks)

Statement of Work

Task 1 *Evaluate phase stability and thermal expansion of candidate perovskite membranes and develop techniques to support these materials on porous metal structures.*

Task 2 *Determine materials mechanical properties under conditions of high temperatures and reactive atmospheres.*

Task 3 *Measure kinetics of oxygen uptake and transport in ceramic membrane materials under commercially relevant conditions using isotope labeling techniques.*

EXECUTIVE SUMMARY

Research on the Oxygen Transport Membranes as listed as tasks 1-3 are being performed at the various universities under the stewardship of Praxair. The quarterly technical report presents the progress of the tasks defined to understand the fundamental concepts and structural performance of the OTM material.

The chemical and structural properties of $La_{0.2}Sr_{0.8}Fe_{0.55}Ti_{0.45}O_{3-\square}$ at 900ºC indicated that space group of R3c yielded a better refinement than a cubic structure of Pm3m. Oxygen occupancy was nearly 3 in the region from room temperature to 700ºC, above which the occupancy decreased due to oxygen loss. Oxygen occupancy refined from R-3c indicated a slight increase in occupancy at 100ºC and oxygen deficiency starts to increase at temperatures higher than 700ºC. The unit cell volume increases with increasing temperature, which is expected due to positive thermal expansion coefficient and generation of oxygen vacancies. The lattice expansion calculated over the temperature region from 100 to 900ºC provided a value of thermal expansion coefficients for *c* and *a* lattice parameters as 16.1 ppm/°C and 15.9 ppm/°C, respectively. The lattice thermal expansion calculated from *in situ* neutron diffraction is ~16ppm/°C. The thermal expansion of L2SF55T is thus assumed to be nearly isotropic.

Dense OTM bars were evaluated for slow crack growth (SCG) in air at room temperature and in condition of flowing N_2 switched to air at 1000ºC. Samples exposed to an environment of N_2 with a switch to Air at 1000ºC indicated that the major XRD peaks had a small but perceptible shift towards the left. The fractured samples indicated a stronger shift towards the left that increased with slower stressing rates. Slow XRD scan rates of fractured samples indicated that the major peaks were no longer single and had decomposed to several peaks. In addition, several additional peaks were indexed with PowderX X-ray analysis program as to Brownmillerite and Aurivilius type of structures. The peaks became dominant in samples fractured at very slow stress rates (~3μm/min). The fracture origins were consistently from the surface and indicated a possible correlation with expansion, decomposition or structural transition of the unit cell of the cubic perovskite structure. The expansion/decomposition and transitions indicate the possibilities of residual stresses which influence crack growth and fracture in the OTM material

The thermal expansion in air for $La_{0.2}Sr_{0.8}Fe_{0.55}Ti_{0.45}O_{3-\delta}$ in the temperature range 25-1200 °C indicated that the expansion of the sample is constant in the isothermal regions and the expansion contraction behavior is reversible. The change of slope in the thermal expansion curve at a temperature ~ 320 °C can be attributed to the onset of oxygen loss upon heating and is in good agreement with the temperature at which the total conductivity is observed to decrease. The change in the chemical expansion is linear with temperature. The expansion coefficient in air in this temperature range is 9.6×10^{-6} K^{-1} while the value obtained at $pO_2 = 2 \times 10^{-4}$atm is smaller at 7.4×10^{-6} K^{-1}. Consequently, the chemical expansion decreases as the temperature increases

Task 1: Preparation and Characterization of Dense Ceramic oxygen Permeable Membranes

X.-D Zhou[1], Q. Cai[2], J. Yang[1], W. B. Yelon[1], W. J. James[1] and H. U. Anderson[1]

1. **Materials Research Center, University of Missouri-Rolla, Rolla, MO 65401**
2. **Department of Physics, University of Missouri-Columbia, Columbia, MO 65211**

In this report, *in situ* neutron diffraction was used to characterize the chemical and structural properties of $La_{0.2}Sr_{0.8}Fe_{0.55}Ti_{0.45}O_{3-\square}$ (here after as L2SF55T) specimen, which was subject to measurements of neutron diffraction from room temperature to 900ºC. It was found that space group of R3c yielded a better refinement than a cubic structure of Pm3m. Oxygen occupancy was nearly 3 in the region from room temperature to 700ºC, above which the occupancy decreased due to oxygen loss.

Experimental

L2SF55T specimen was sintered at 1400ºC for 2 hours and then cooled to room temperature at 3ºC/min. The bar sample with a geometry ~35mmx3mmx3mm was hung in the high temperature furnace which was designed to conduct *in situ* neutron diffraction measurements. Two runs were performed from room temperature to the elevated temperature. During the first run, the sample was heated to 500ºC and cooled to room temperature. The specimen was heated up to 900ºC during the second run. The neutron measurements were carried out using the position sensitive detector – diffractometer at the University of Missouri Research Reactor (MURR) in Columbia, MO. For Neutron Diffraction (ND) studies, samples were contained in 3 mm V metal cells and data were collected at 1.4785 Å over a range of 5º-105º (2θ). Rietveld refinement was carried out using the FULLPROF code, in which the magnetic ordering was taken into account because of the sensitivity of neutron diffraction to the magnetic ordering of the Fe atoms.

Results and Discussion

Unlike the specimens of $La_{0.6}Sr_{0.4}FeO_{3-\delta}$ (L6SF), there was no evidence for antiferromagnetic ordering in the diffraction data, i.e., the observed data could be fully fitted without any magnetic contribution. In our previous quarterly report, we showed that a higher symmetry space group could be used in comparison to L6SF (the P-3/c1 group). We employed a space group of R-3c for the quenched samples and observed that

$c/2\sqrt{3}$ was nearly the same as $a/\sqrt{2}$, which indicated a cubic space group (Pm3m) may be a suitable space group for refinement. In this report, therefore, we are intent to compare the refinements from Pm3m and R-3c.

Table 1 and 2 show parameters refined from *in situ* neutron diffraction measurements. Fig. 1 shows a plot of $c/2\sqrt{3}$ and $a/\sqrt{2}$ as a function of measuring temperature for those measurements. Space group of R-3c resolved a better refinement and was then used for *in situ* neutron diffraction data analysis.

Fig. 2 shows oxygen occupancy and unit cell volume as a function of measuring temperature refined from Pm3m. Oxygen excess was observed from room temperature to 800ºC and the data scattered over a wide range of oxygen occupancy. Fig. 3 shows oxygen occupancy and unit cell volume as a function of temperature, which were refined from R-3c. The slight increase of oxygen occupancy at 100ºC could have resulted from the absorption of oxygen. Similar behavior has been observed in some other perovskites. As can be seen oxygen deficiency starts to increase when the measuring temperatures are higher than 700ºC. The unit cell volume increases with increasing temperature, which is expected due to positive thermal expansion coefficient and generation of oxygen vacancies. Fig. 4 illustrates plots of a and c as a function of measuring temperature. The lattice expansion can be calculated over the temperature region from 100 to 900ºC. Slope values of 0.000218 and 0.0000882 were observed for c and a vs. T respectively. The thermal expansion coefficients for c and a lattice parameters were found to be 16.1 ppm/°C and 15.9 ppm/°C, respectively. Hence, thermal expansion of L2SF55T is nearly isotropic.

The average volume expansion coefficient α over the measuring temperature range is related to the linear expansion coefficient by:

$$1+\alpha\Delta T = 1+3a\Delta T+3a^2\Delta T^2+a^3\Delta T^3$$

where a is the linear expansion coefficient. From Fig. 3, a slope value of 0.01743 was observed over the temperature region from 100 to 900ºC, which yields $\alpha \sim 48.58$ ppm/°C. Since a is small, $\alpha = 3a$ is a good approximation, which yields a values of $a \sim 16.2$ ppm/°C. Therefore, the lattice thermal expansion calculated from *in situ* neutron diffraction is ~16ppm/°C.

Table 1. L2SF55T Bulk sample at high temperature, air, cubic Pm-3m, La/Sr=0.042/0.167. Fe/Ti=0.112/0.096

1st run:

Temp C	B(A)	SB(A)	B(B)	SB(B)	B(O)	sB	Occ(O)	sOcc	a	sa	Vol	sVol
RT	1.261	58	0.834	121	1.732	44	0.601	5	3.90404	11	59.504	3
97	1.750	56	1.018	79	2.270	44	0.612	5	3.90762	12	59.667	3
200	1.876	51	1.112	72	2.378	40	0.611	4	3.91108	11	59.826	3
297	2.123	58	1.339	82	2.569	45	0.610	4	3.91739	12	60.116	3
398	2.232	59	1.458	83	2.736	45	0.613	4	3.92237	12	60.345	3
501	2.407	62	1.647	87	2.943	47	0.615	5	3.92767	12	60.590	3

2nd run:

Temp C	B(A)	SB(A)	B(B)	SB(B)	B(O)	sB	Occ(O)	sOcc	a	sa	Vol	sVol
RT	2.047	49	0.972	66	2.438	40	0.607	4	3.90093	12	59.361	3
97	1.118	56	0.543	81	1.753	45	0.616	5	3.91137	12	59.839	3
198	1.292	59	0.714	86	1.891	46	0.615	5	3.91681	12	60.089	3
294	1.475	60	0.879	86	2.081	47	0.616	5	3.92221	12	60.338	3
401	1.569	64	0.875	90	2.146	50	0.614	5	3.92820	13	60.615	3
504	1.819	69	1.239	100	2.362	52	0.613	5	3.93441	14	60.903	4
598	1.767	67	1.141	96	2.451	51	0.617	5	3.94033	13	61.178	4
696	1.924	70	1.295	100	2.793	55	0.626	5	3.94601	28	61.443	7
798	2.173	76	1.649	111	2.989	59	0.617	6	3.95336	31	61.788	8
891	2.730	74	2.086	105	3.291	56	0.602	5	3.96062	32	62.128	9

Table 2. Refined with r-3c and oxygen is at 36f only:

1st run: occ(La)/Sr=0.033/0.133, Fe/Ti=0.09/0.077

Temp	a	c	x(o)	y(o)	z(o)	B(A)	B(B)	B(o)	Occ(o)	socc	Vol	svol	χ^2
RT	5.52399(20)	13.50302(101)	0.4988(9)	0.008(1)	0.2352(5)	1.16(5)	0.9(1)	0.64(7)	0.484	4	356.835	32	7.94
97	5.52896(21)	13.51706(106)	0.502(1)	0.012(1)	0.2351(5)	1.61(5)	1.12(7)	1.17(7)	0.496	3	357.849	34	2.86
200	5.53403(21)	13.52933(99)	0.504(1)	0.015(2)	0.2374(6)	1.76(5)	1.20(7)	1.52(6)	0.492	3	358.831	32	2.30
297	5.54288(20)	13.54880(102)	0.504(1)	0.014(1)	0.2353(5)	1.99(5)	1.42(7)	1.44(7)	0.492	3	360.498	33	2.55
398	5.54990(23)	13.56616(117)	0.505(2)	0.016(2)	0.2359(6)	2.10(5)	1.56(8)	1.67(7)	0.494	3	361.874	38	2.50
501	5.55730(23)	13.58562(117)	0.508(6)	0.016(2)	0.2360(6)	2.29(6)	1.75(8)	1.89(8)	0.495	3	363.361	38	2.37

2nd run: occ(La)/Sr=0.033/0.133, Fe/Ti=0.09/0.077

Temp	a	c	x(o)	y(o)	z(o)	B(A)	B(B)	B(o)	Occ(o)	socc	Vol	svol	χ^2
RT	5.51886(43)	13.49961(216)	0.502(2)	0.014(3)	0.238(1)	1.96(5)	1.05(6)	1.7(1)	0.488	2	356.082	69	6.24
97	5.53433(25)	13.53199(121)	0.502(1)	0.014(2)	0.2374(7)	0.99(5)	0.63(8)	0.90(8)	0.498	3	358.941	39	3.10
198	5.54184(26)	13.55118(130)	0.505(3)	0.012(2)	0.2361(7)	1.18(6)	0.81(8)	0.90(9)	0.496	3	360.426	42	3.13
294	5.54958(26)	13.56964(129)	0.51(1)	0.015(2)	0.2371(7)	1.36(6)	0.99(8)	1.19(8)	0.497	3	361.926	42	2.92
401	5.55826(25)	13.58761(127)	0.510(2)	0.014(2)	0.2364(7)	1.45(6)	0.97(8)	1.17(9)	0.495	4	363.539	41	2.97
504	5.56681(27)	13.60917(139)	0.507(5)	0.013(2)	0.2357(7)	1.71(6)	1.31(9)	1.29(9)	0.494	4	365.237	45	2.93
598	5.57509(30)	13.63258(152)	0.511(2)	0.017(3)	0.2374(9)	1.68(6)	1.25(9)	1.54(9)	0.497	4	366.954	50	2.52
696	5.58472(35)	13.65723(179)	0.510(4)	0.017(3)	0.237(1)	1.84(7)	1.46(9)	1.8(1)	0.497	4	368.889	58	2.65
798	5.59583(34)	13.68131(178)	0.509(3)	0.015(2)	0.2354(9)	2.12(7)	1.8(1)	1.8(1)	0.491	4	371.012	58	2.80
891	5.60397(37)	13.70493(198)	0.51(3)	0.019(3)	0.236(1)	2.68(7)	2.2(1)	2.1(1)	0.478	3	372.734	64	2.41

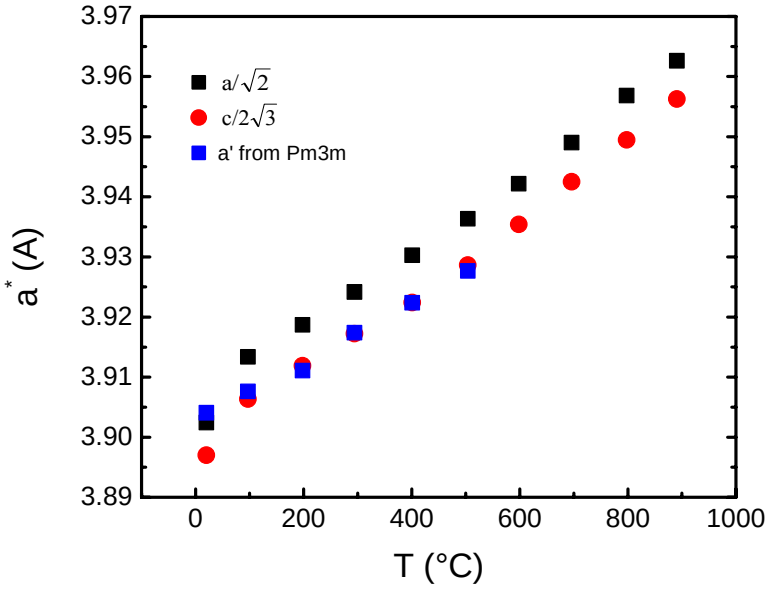

Fig. 1. a^* as function of measuring temperature for *in situ* neutron diffraction, where a' was refined fro Pm3m and other two were refined from R3c.

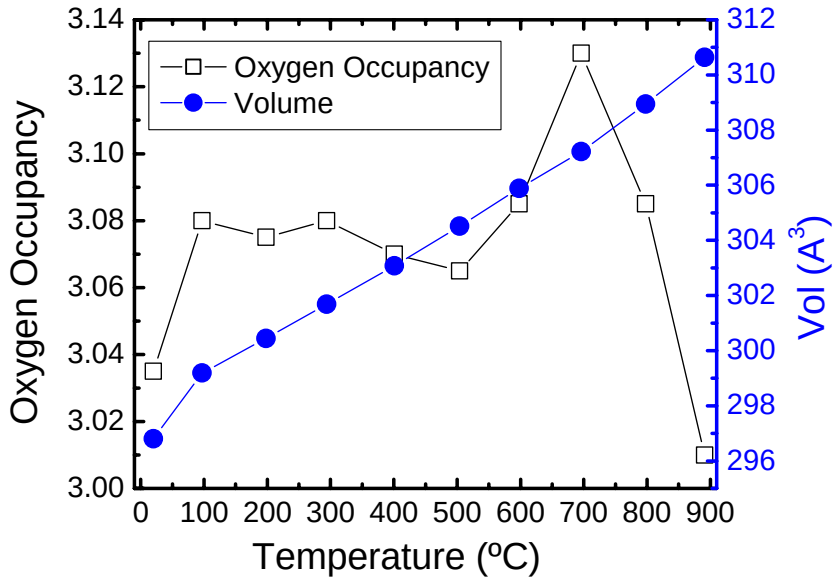

Fig. 2. Oxygen occupancy and unit cell volume as a function of measuring temperature, in which data were refined from space group of Pm3m.

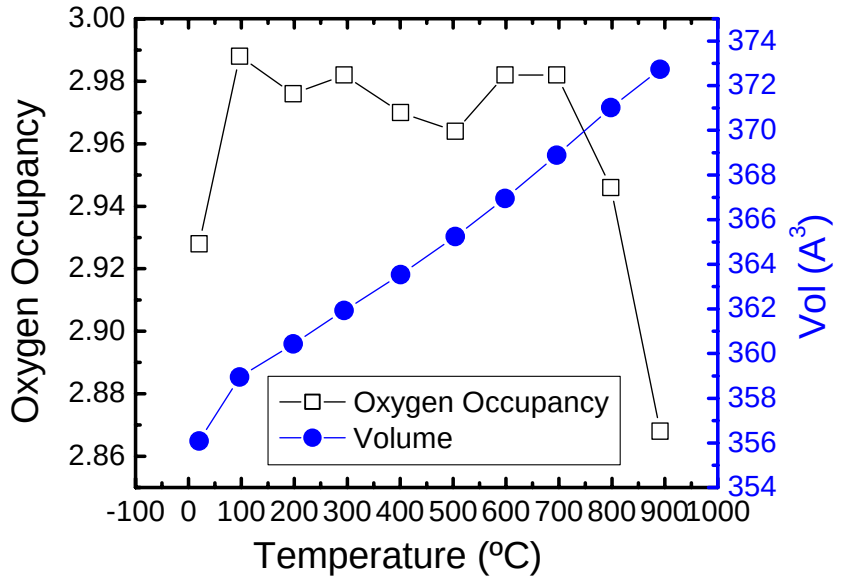

Fig. 3. Oxygen occupancy and unit cell volume as a function of measuring temperature, in which data were refined from space group of R3c.

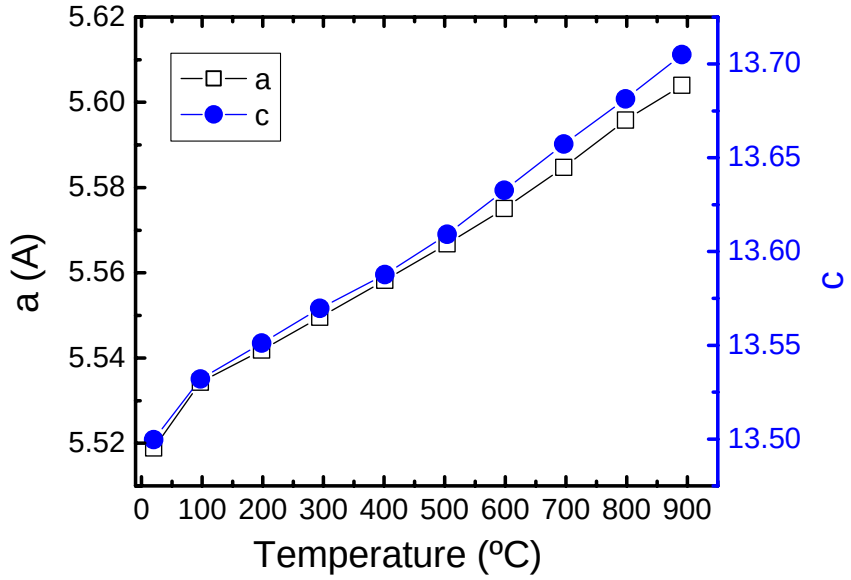

Fig. 4. Lattice parameter (a and c) as a function of measuring temperature, in which data were refined from space group of R3c.

TASK 2: Determine material mechanical properties under conditions of high temperature and reactive atmosphere

Prof. Sukumar Bandopadhyay and Dr. Nagendra Nagabhushana

University of Alaska Fairbanks

In this quarter, studies were continued on OTM bar samples received from Praxair. Samples fractured in slow crack growth tests were analyzed in a XRD and SEM for phase composition and fracture mechanism respectively.

EXPERIMENTAL

In the previous quarter, 21 OTM bars of dimensions 3x4x48 mm provided by Praxair were tested for slow crack at 1000ºC in an atmosphere of N_2/Air respectively. The fractured surfaces were cut from the failed surfaces and sputtered with gold for fracture analysis. In addition, samples were cut near to fracture, powdered and analyzsed in XRD for information on phase retention or precipitation of secondary phases. The XRD were done under two conditions – a fast scan to provide complete data and a slow scan with a step angle of 0.01 degrees and a dwell time of 2 secs. In both the conditions, the XRD was operated at 30 KV and 20 mA with a Cu target.

RESULTS AND DISCUSSIONS

XRD Analysis

The full scale and the relevant peak XRD analysis are shown in figure 1 and 2 respectively. The following observations were made on the data obtained:

1. The as-received OTM samples indexing to a primitive cubic perovskite structure with a lattice parameter of **$3.9105A^o$**.
2. Samples exposed to an environment of N_2 with a switch to Air at 1000ºC indicated that the major XRD peaks had a small but perceptible shift towards the left. In the sample exposed to air at 1000ºC, the shift was to the right.
3. There were no significant decomposition peaks in the samples exposed to N_2/Air or to air at 1000ºC
4. In the samples fractured in the environment, the major XRD peaks shift towards the left. The shift (to the left) was higher in samples fractured with slower stressing rates.

5. Slow XRD scan rates of fractured samples indicated that the major peaks were no longer single and had decomposed to several peaks. In addition, several additional peaks were becoming dominant.
6. Much of the peaks were indexed with ICDD and ICSD database and had a close match corresponding to $La_2SrFe_2O_7$, $LaSrFeO_4$, $LaSr_3Fe3O_{9.9}$, $LaFeO_3$, $SrCrO_3$ $Sr_3Cr_2O_7$, $CrFeSr_2O_{5.544}$, $Sr_3Fe_2O_6$, Sr_2FeO_4, $Sr_3Fe_2O_{6.93}$ and $Sr_2Fe_2O_5$ phases. However, there were also some peaks which couldn't be index at all.
7. Some of the unexplained peaks were indexed with PowderX X-ray analysis program to Brownmillerite (or $Sr_2Fe_2O_5$ type phases) and Aurivilius type of structures. In earlier electron microscopy studies on LaSrFeCrO at UIC, these structures were analyzed to be of the following lattice parameters

   Phases: P = Perovskite, B= Brownmillerite, A = Aurivilius)

   Lattice Parameter of Perovskite ($\mathbf{a_c}$) = **3.9105*A*^{o}**

   Brownmillerite Phase

   $a_0 = a_c$*sqrt(2) = 5.5352

   $b_0 = 3a_c$ = 11.742 $c_0 = a_c$*sqrt(2) = 5.5352

   Aurivilius phase:

   a_0=sqrt(20)*a_c = 17.4878

   b_0=0.97*a_c = 3.7930 c_0=sqrt(20)*a_c = 17.4878

8. In sample fractured at very slow stress rates (~3micron/min), the brownmillerite ($Sr_2Fe_2O_5$ type) peaks became more dominant.

The X-Ray data and the observations points to non-equilibrium decomposition of the LSFCO OTM membrane. The non-equilibrium conditions could probably be due to the nature of the applied stress field (stressing rates) and leads to transition in crystal structures and increased kinetics of decomposition. The formations of a Brownmillerite or $Sr_2Fe_2O_5$ type structures, which are orthorhombic are attributed to the ordering of oxygen vacancies. The cubic to orthorhombic transitions leads to 2.6% increase in strains and thus residual stresses generated could influence the fracture behavior of the OTM membrane.

On a cautious note, the interpretation of the data has to be backed by simulation of the XRD profiles and physical evidence of the ordering or phase transitions. For this work has begun on using X-ray diffraction programs such as FULLPROF in refining the possible structures and crystal geometry.

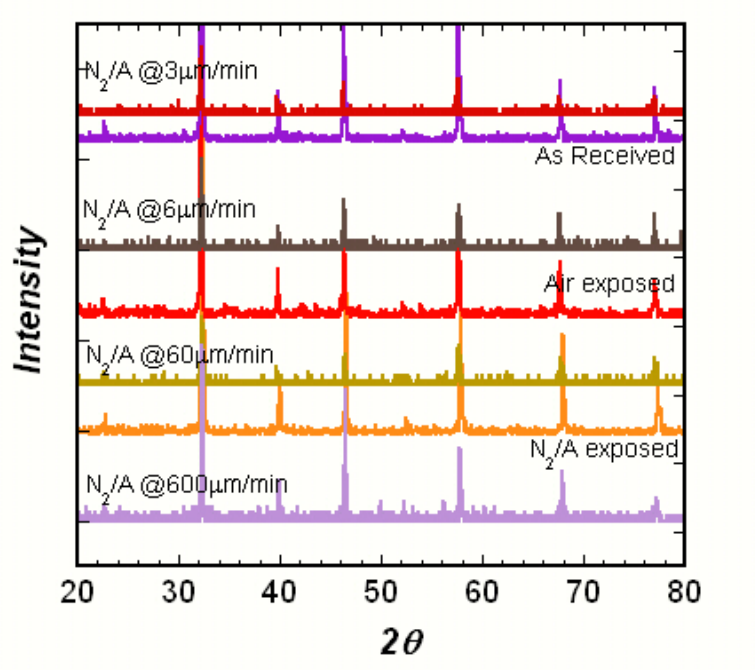

Fig. 5 XRD plots of the OTM samples in a) as received, b) exposed to Air at 1000ºC; c) exposed to N_2/Air at 1000ºC and fractured at varying stress rates in N_2/Air at 1000ºC

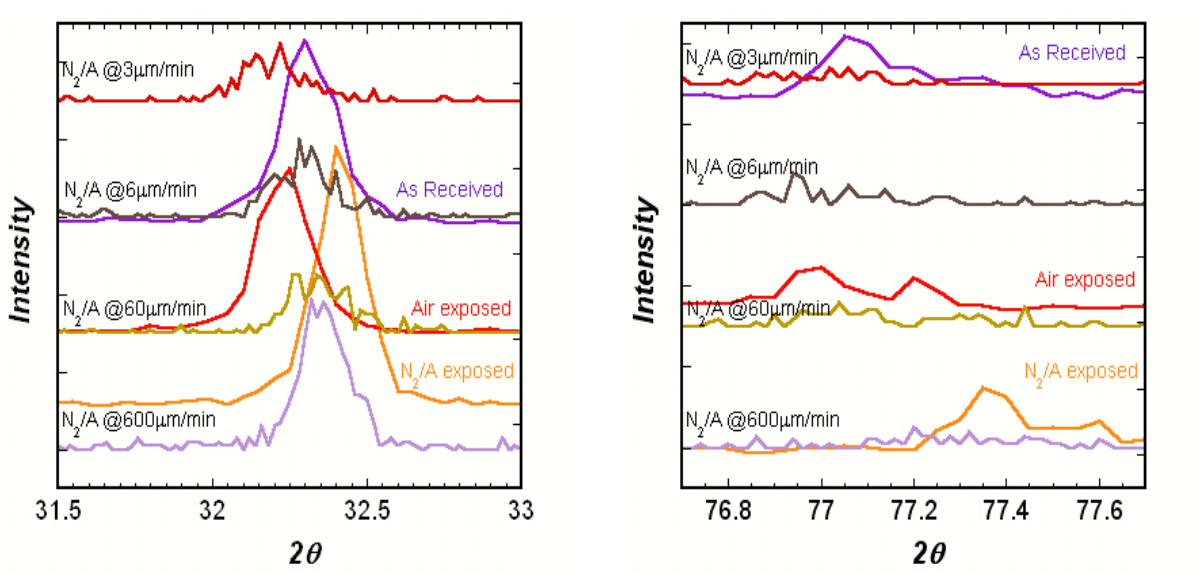

Fig. 6 XRD of the major peaks (2Theta = 32 and 77) plots of the OTM samples indicating a perceptible shift and decomposition of the single peaks.

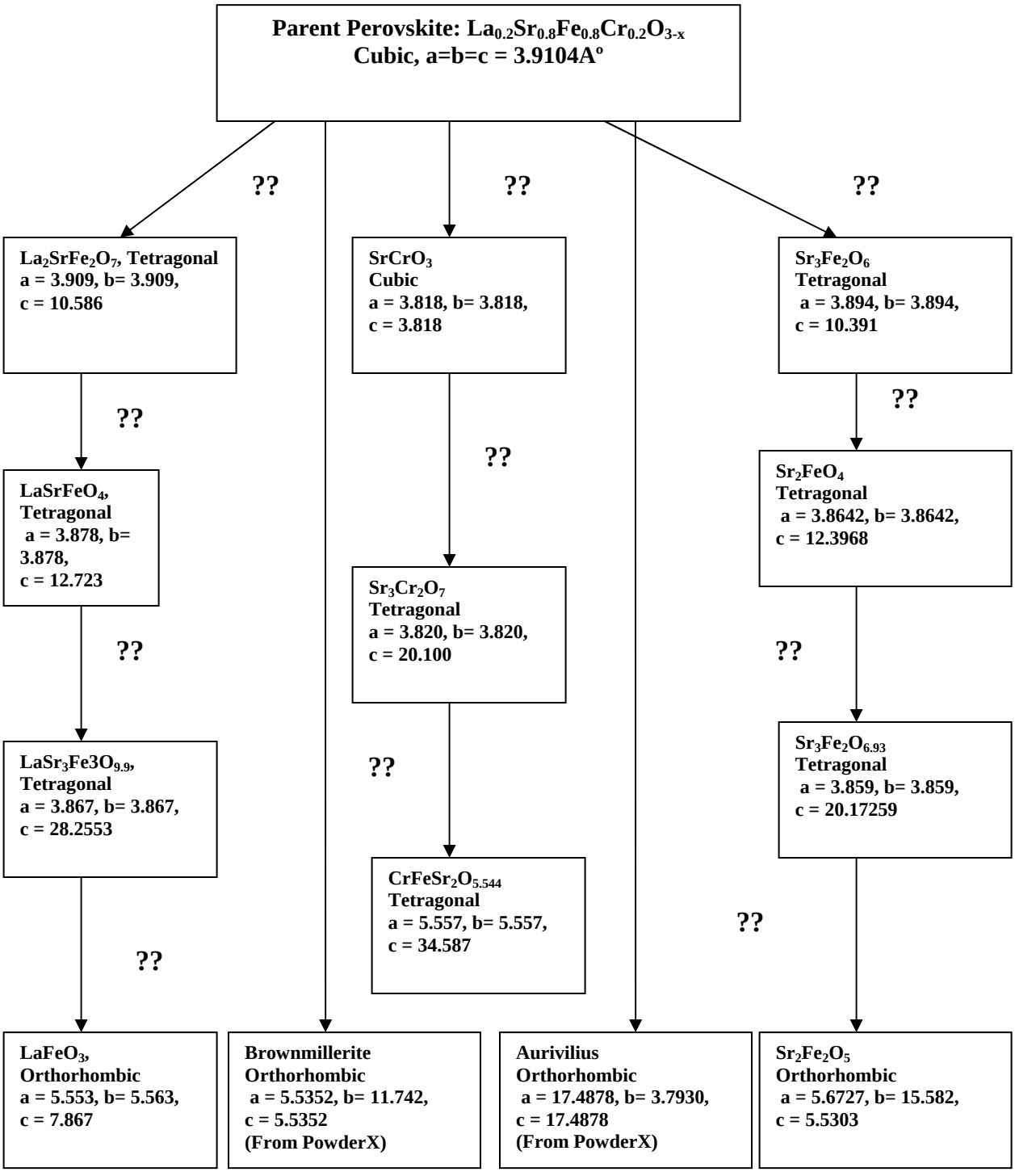

Based on the data available from the X-ray analysis of OTM fractured samples, a tentative flow chart indicating a possible decomposition route is created. The significance of this on fracture and crack growth behavior is studied.

Fracture analysis

The fractured samples were sectioned in a low speed saw and the surfaces sputtered with gold prior to examination in an electron microscope.

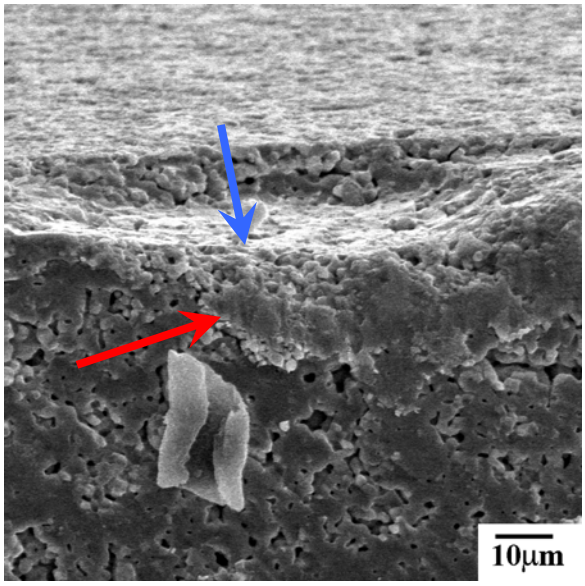

Fig. 7: Surface flaw as fracture origin

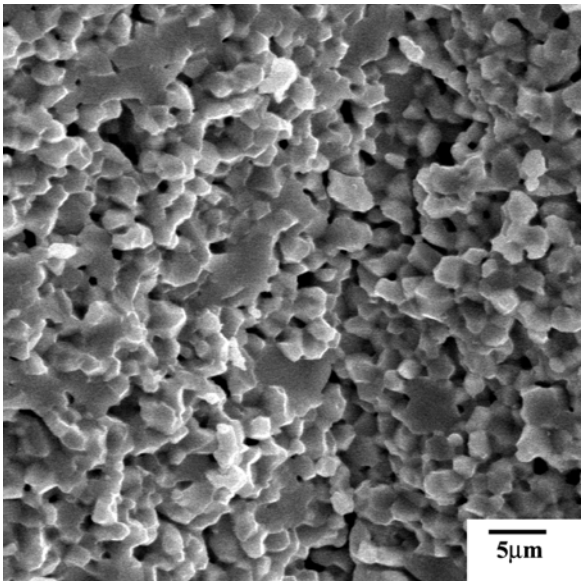

Fig. 8: Intergranular fracture in OTM bars

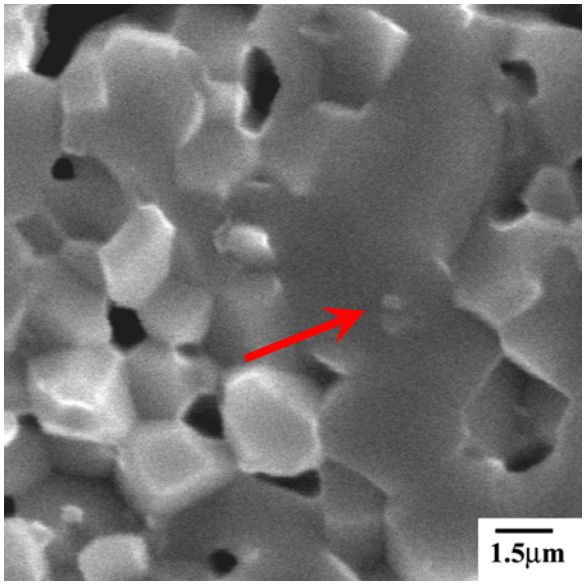

Fig. 9a: Intergranular fracture of grains along with presence of fine precipitates

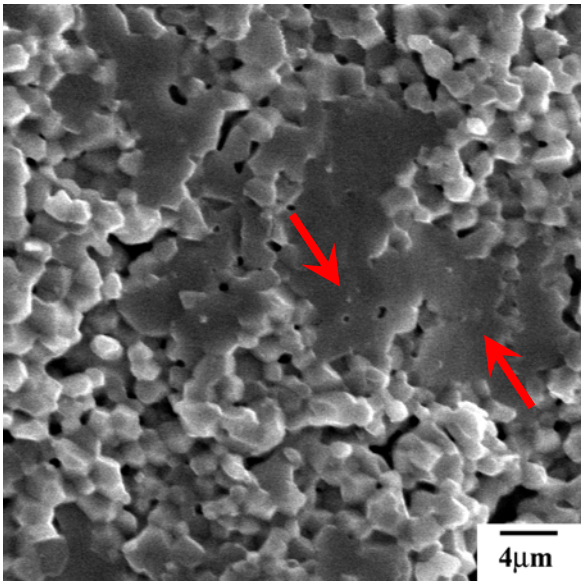

Fig. 9b: Trans/Intergranular fracture in OTM and formation of fine precipitates

In all the samples analyzed, the fracture origins were consistently from the surface (Fig. 7) which led to a conclusion that fracture strength were controlled by surface condition. The surface were ground and finished by researchers at Praxair.

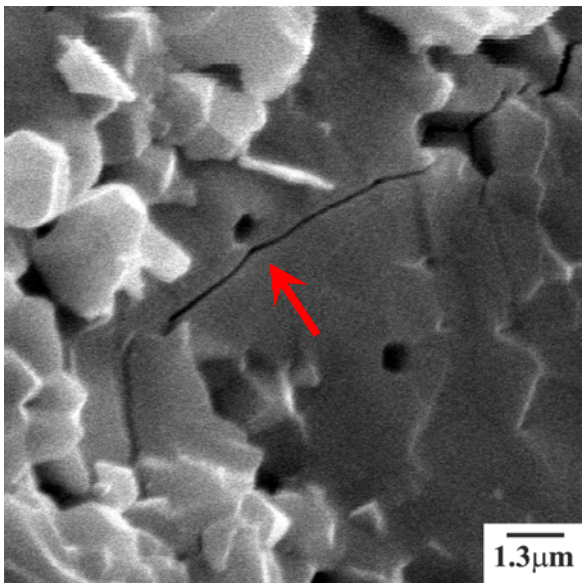

Fig.10: Interaction of microstructure with secondary cracks. Increased formation of precipitates is observed

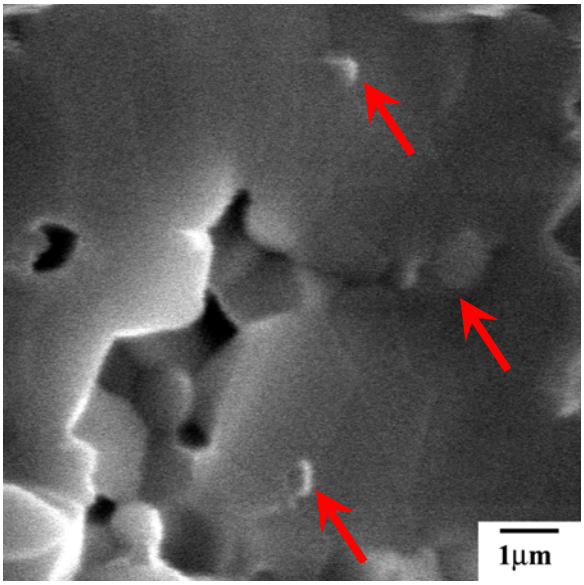

Fig.11: Transgranular fracture and presence of two types of precipitates

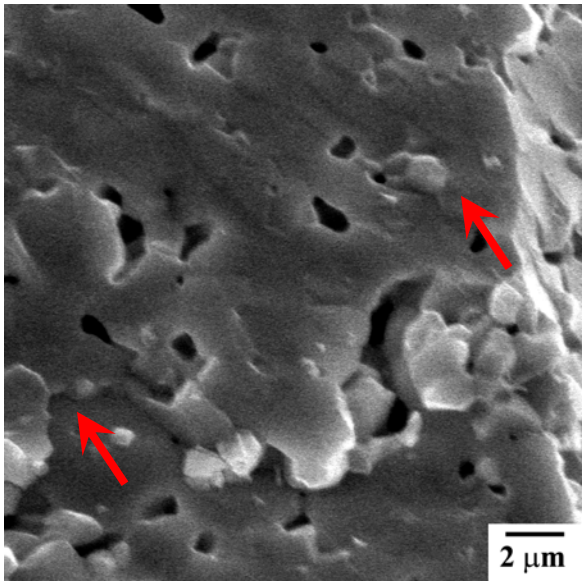

Fig.12: Slow transgranular crack growth with increased formation of two types of precipitates

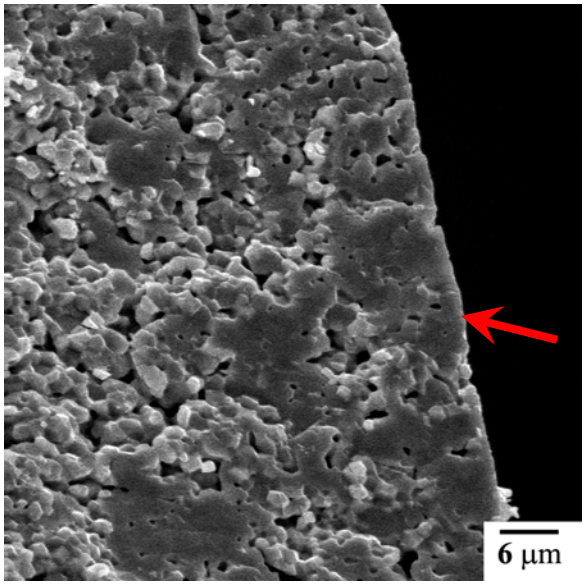

Fig.13: Fast Transgranular fracture at the edge. The so called compressive curl consistently leads to transgranular fracture

Initial scanning of the fracture surfaces indicated an intergranular mode of fracture. However, several nuances were observed depending on the position in the fractured samples.

1. The area very near (~5-10 micron in Fig. 7) to the tensile surface of the flexure bar was predominantly of intergranular fracture. The fracture originates from surface flaws (blue arrow) and proceeds along the grain boundaries. The cracks coalesce and proceed in a transgranular mode through the OTM grains (red arrow). Precipitation of secondary phases are also observed (Fig. 9). Fracture away from the tensile surface was a mix of intergranular and transgranularly failed grains (Fig. 9b). The region of transgranular failure increased with slower stress rates and corresponded with increased formation of fine precipitates.
2. The interaction of the crack with the microstructure was better illustrated in the secondary cracks. As shown in Fig. 10, the secondary cracks have followed a transgranular mode through the OTM grains. The secondary cracks were observed very close to the transition from intergranular to transgranular modes of fracture and indicated the possible presence of localized residual stresses. Residual stresses can alter the trajectory of the crack paths in the OTM structures. Regions of transgranularly fractured grains also indicated increased formation of precipitates. As shown in Fig 11, two distinct precipitates: a coarse (~ 0.5 -0.8μm) and very fine (0.1-0.25μm) were observed to form at the grain boundary and grain boundary junctions.
3. As reported in earlier studies on OTM batches, crack growth was transgranular irrespective of the environmental condition. However, in the present OTM materials crack growth was a mix of intergranular and transgranular mode. In the region from the tensile to the neutral axis, crack growth was predominantly intergranular with isolated pockets of transgranular fracture. In the areas away from the neutral axis and extending toward the compressive side (back side of the flexure bar), increased pockets of transgranular fracture along with increased formation of secondary precipitates were observed (Fig. 12). Interestingly as shown in Fig. 13, grains at the compressive side failed in a transgranular mode. Moreover, these were also the region of fast fracture and correlated well with increase in area of transgranular fracture increased with decreased applied stress rates.

Fracture analysis in combination with X-ray analysis indicate a possible correlation with expansion, decomposition or structural transition of the unit cell of the cubic perovskite structure. The expansion/decomposition and transitions indicate the possibilities of residual stresses which influence crack growth and fracture in the OTM material. This needs to be further addressed by careful experimentation and modeling of the residual stresses. The next quarter will have more detailed analysis in identifying the transitions in crystal structure, the nature of the stresses developed and their influence on crack growth. For this several commercial software such as FEMLAB along with other software such as CAST3M has been acquired to model thermal expansion etc.

Task 3: Measurement of Surface Activation/Reaction rates in Ion Transport Membranes using Isotope Tracer and Transient Kinetic Techniques.

Prof. Alan Jacobson, University of Houston/University of Toronto

University of Houston
Conductivity and Thermodynamic Studies

We have continued to investigate the thermodynamic properties (stability and phase-separation behavior) and total conductivity of prototype membrane materials. The data are needed together with the kinetic information to develop a complete model for the membrane transport. We have previously reported characterization, stoichiometry and conductivity measurements for samples of $La_{0.2}Sr_{0.8}Fe_{0.55}Ti_{0.45}O_{3-x}$. In this report, we describe measurements of the chemical and thermal expansion as a function of temperature and pO_2.

Dilatometry Experiments

Rectangular sample bars (14.38 mm × 4.47 mm × 5.33 mm) were sintered at 1450 °C for 10 h for use in dilatometry measurements (NETZSCH, DIL 402C). Thermal expansion measurements were performed at 25 ≤ T ≤ 1200 °C with a heating and cooling rate of 3 °C per minute. Purified air was flowed through the dilatometer furnace at ~80 ml/min. Chemical expansion data for the sample were obtained by switching the gas from air to pure argon or to a specific gas mixture (5% H_2/N_2, CO_2, and argon) in the temperature range between 800 and 1000 °C. The flow rate of the each gas was controlled by using mass flow controllers (MKS 247C). An oxygen analyzer (AMETEK, TM-1B) was connected to the dilatometer. The oxygen partial pressures (pO_2) were recorded every minute by measuring the emf reading of an oxygen analyzer using an HP 3468A multimeter.

Fig. 14(a) shows the thermal expansion data in air for $La_{0.2}Sr_{0.8}Fe_{0.55}Ti_{0.45}O_{3-\delta}$ in the temperature range 25 ≤ T ≤ 1200 °C. The measurements were made with a heating and cooling rate of 3 °C per minute. The expansion of the sample is essentially constant in the isothermal regions as expected an the expansion contraction behavior is reversible. The sample expansion with increasing temperature as shown in Fig. 14(b) and four dilatometric curves indicate very good reproducibility. The change of slope in the thermal expansion curve at a temperature ~ 320 °C can be attributed to the onset of oxygen loss upon heating. This temperature is in good

agreement with the temperature at which the total conductivity is observed to decrease in DC conductivity measurements and the onset of the weight loss in TGA experiments.

Based on these dilatometry results, the average thermal expansion coefficients (TECs) can be calculated as follows:

$$\alpha_i = \underset{T_t \to T_0}{Limit} \frac{L_t - L_0}{L(T_t - T_0)} = \frac{1}{L}\frac{dL}{dT} \qquad (2)$$

where α_i is the coefficient of linear thermal expansion per degree. L_t and L_0 are the specimen length at temperature T_t and T_0 respectively and dL/dT is the slope of the length-temperature curve.

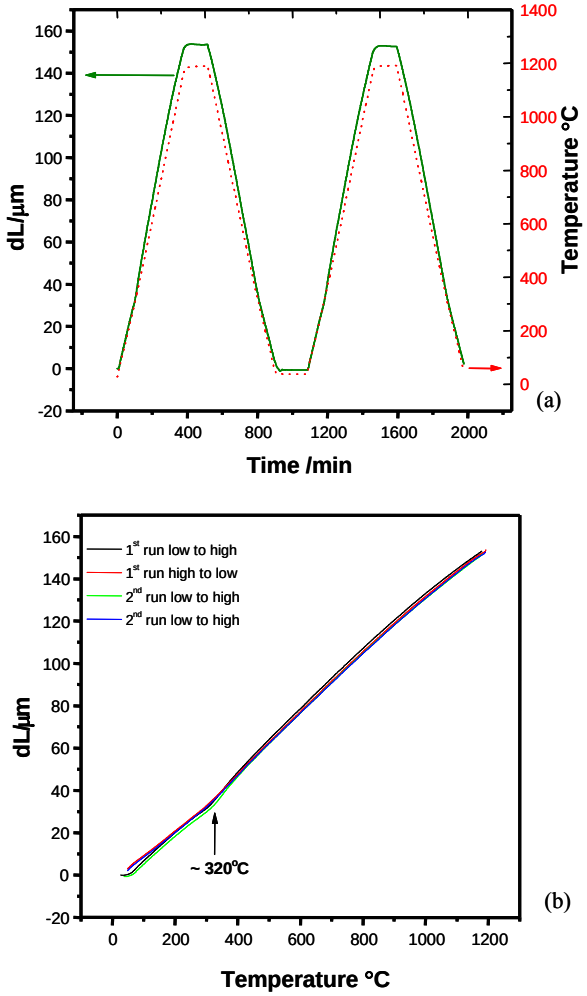

Figure 14 Dilatometry data for $La_{0.2}Sr_{0.8}Fe_{0.55}Ti_{0.45}O_{3-\delta}$ (a) dL vs. time and (b) dL vs. temperature. The dotted line in a indicates the temperature profile.

The average TEC of $La_{0.2}Sr_{0.8}Fe_{0.55}Ti_{0.45}O_{3-\delta}$ is ~ 10×10^{-6} K^{-1} which is similar to that of yttria-stabilized zirconia (~ 10.7×10^{-6} K^{-1}) at elevated temperature. The maximum change of length is 154.6 μm (1.07%) in the measured temperature range.

Chemical expansion data for $La_{0.2}Sr_{0.8}Fe_{0.55}Ti_{0.45}O_{3-\delta}$ were obtained at $800 \leq T \leq 1000$ °C and at ~ $10^{-4} \leq pO_2 \leq 0.21$ atm in the following way. The sample was first heated to 800 °C in air and the total expansion measured. The temperature of the sample was then held at 800 °C to reach a constant length (see Fig. 15a). At this point, the gas was switched from air to argon leading to chemical expansion of the sample due to loss of oxygen. The pO_2 was monitored and the conditions maintained until no further change in length occurred. Constant length is obtained after ~ 220 min with a length change of ~ 28.43 μm. After several hours, argon gas is switched back to air in order to determine the degree and the rate of contraction. The amount of contraction agrees well with the expansion but equilibrium is achieved occurs ~ 83 min suggesting that the reaction rate is at least three times faster. The experiment was then repeated at temperatures from to 850 to 1000 °C in 50 °C increments with similar results (see Fig. 15a). Flow rates of 80 ml/min of air and argon ($pO_2 = 2 \times 10^{-4}$ atm) were used in the experiment and the switch time from argon to air is limited by the time it takes to switch out the gas (see Fig. 15b). The present experiment is not designed to extract reliable kinetic data because of the long switch out time. Faster equilibration times and smaller changes in length were observed as the temperature was increased.

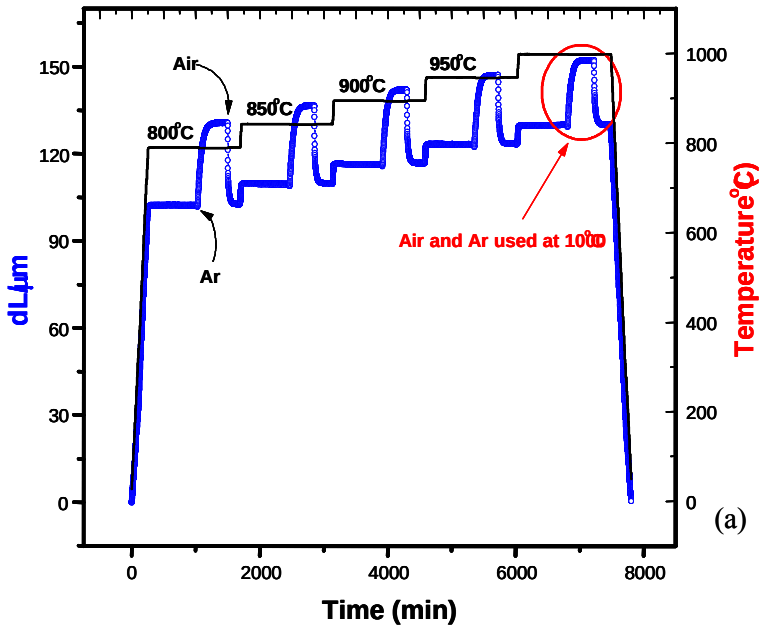

Figure 15(a) Chemical expansion data for $La_{0.2}Sr_{0.8}Fe_{0.55}Ti_{0.45}O_{3-\delta}$ - dL vs. time for the switch at 1000 °C.

The temperature dependence of the total expansion coefficient was extracted from the data in Figure 15a at the two conditions (pO2 = 0.21 and 2×10^{-4} atm) and the are shown in Figure 3a. The change in the chemical expansion is linear with temperature. The expansion coefficient in air in this temperature range is 9.6×10^{-6} K^{-1} while the value obtained at $pO_2 = 2 \times 10^{-4}$atm is smaller at 7.4×10^{-6} K^{-1}. Consequently, the chemical expansion decreases at the temperature increases as shown in Figure 16b.

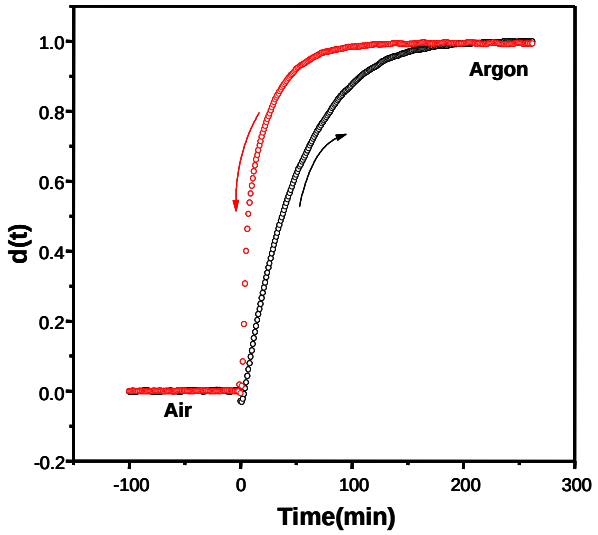

(b)

Figure 15b Chemical expansion data for $La_{0.2}Sr_{0.8}Fe_{0.55}Ti_{0.45}O_{3-\delta}$ - relative dL vs. time for the switch at 1000 °C.

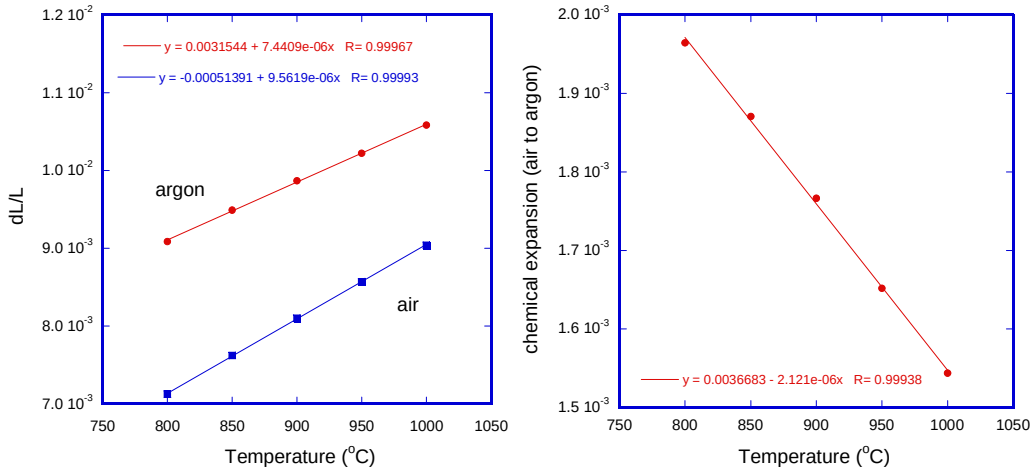

Figure 16(a) Expansion of $La_{0.2}Sr_{0.8}Fe_{0.55}Ti_{0.45}O_{3-\delta}$ in air and argon, the difference between the two lines is the chemical expansion on changing from $pO_2 = 0.21$ atm to 2×10^{-4} atm; (b) the change in chemical expansion with temperature.

University of Toronto

Isotope Transient Studies Through a Dense Membranes

Summary of experimental progress:

Our last report described the end of experiments on $La_{0.6}Sr_{0.4}Co_{0.2}Fe_{0.8}O_{3-\delta}$ (LSCF-6428) and the beginning of experiments on a new membrane of $La_{0.2}Sr_{0.8}Cr_{0.2}Fe_{0.8}O_{3-\delta}$ (LSCrF-2828). During the past quarter we have done the following:

LSCF-6428 study: We are continuing the analysis of data from the LSCF-6428 study. For the quenched membrane data, we have reanalyzed regions of the quenched membrane with better resolution and signal/noise. We have also written data manipulation codes which allow us to retrieve isotope profiles from the SIMS data obtained on the tubular membrane geometry. Various profiles will be analyzed with this new data set to study the radial variability of the diffusivity in the quenched membrane.

LSCrF-2828 studies: A series of isotope transients under air separation mode (small gradient) were completed on the membrane of LSCrF-2828 at 900°C. Furthermore, a low pO_2 atmosphere has been successfully admitted to the delivery side of the LSCrF-2828 membrane and we obtained several transients in a "model syngas" mode with CO/CO_2 on the fuel side. At low CO partial pressures, two modes of oxygen delivery to the fuel side of the membrane were observed

(1) Recombination to form molecular oxygen was observed, even in the presence of carbon monoxide in the fuel-side gas phase.
(2) Carbon monoxide oxidation to form CO_2 was also observed.

Thus, these two processes can proceed simultaneously with comparable rates. This is in agreement with our previous IEDP results which show that the redox part of isotope exchange in CO_2/CO atmospheres (related to CO oxidation) is comparable in rate on this material. The critical part played by the surface oxidation state in the rates on an operating membrane is revealed in these current experiments.

As the CO pressure is increased, the CO oxidation rate is capable of intercepting a greater fraction of the transported oxygen, until no detectable molecular oxygen was observed. At this point, the membrane flux is also much increased, due to the increase in chemical potential across the membrane. Thus, we have sampled a wide range of chemical gradients in the isotope transient experiments in this membrane.

At the end of these experiments, we quenched the LSCrF-2828 membrane in a manner similar to the LSCF-6428 membrane. A visiting student from Technical University, Munich, Stefan

Gruber, who arrived in February, has obtained the first analyses of this sample and also improved our 2-D model. A small leak had opened just before this quench experiment, and the sample was damaged during removal. However, meaningful profiles were obtainable from the fragments. This analysis is ongoing. We will also analyze an axial section to examine the evolution of the profile along the direction of gas flow. The chemical potential may have substantial changes in the axial direction, since the inlet was pure CO for the quench experiment.

Personnel changes: During the past quarter, Dr. Linjie Hu has left the group to take up another position after 2.5 years in my lab. This had been expected, but the timing uncertain. His replacement is being sought and several good candidates are available.

CONCLUSIONS

For a detailed analysis of the transport properties Ti doped LSF further studies are need to be by *In situ* neutron diffraction. Presently, the space group of R3c yields a better refinement than a cubic structure of Pm3m. The oxygen occupancy is observed to be nearly 3 in the region from room temperature to 700ºC, above which the occupancy decreased due to oxygen loss. These have implication on the thermal expansion of the crystal and needs to be correlated with physical measurements on Ti doped LSF.

Fracture in LSFCO-OTM material is depended on the applied stress rates. Although, fracture is predominantly intergranular, pockets of transgranular fractures is observed. Transgranular fracture appears to have a correlation with the localized stresses fields and also on the decomposition of the parent perovskite material. Further experimental evidence and modelling needs to be carried to gain conclusive evidences.

Studies extended on the $La_{0.2}Sr_{0.8}Fe_{0.55}Ti_{0.45}O_{3-x}$ samples included measurements of the chemical expansion over a wider range of p_{O2}. The measurements of electrical conductivity relaxation to determine the diffusion and the surface exchange coefficients were postponed to do the dilatometry but will be started in the next quarter. Data collection for the past few months has stopped at a cursory stage to assures us of better quality of the data and allow initial evaluation of trends to guide the experiments and to suggest experiments to complete a give set and guard against omissions of important experiments. The tools developed for analyzing the isotope data obtained in ToFSIMS in the past quarter will be used in this analysis.

REFERENCES

N/A

BIBLIOGRAPHY:

N/A

LISTS OF ACRONYMS AND ABBREVIATIONS:

OTM	Oxygen Transport Membrane
LSFCO	Lanthanum Strontium Iron Chromium Oxide ($La_{0.2}Sr_{0.8}Fe_{0.8}Cr_{0.2}O_{3-\delta}$)
LSF	Lanthanum Strontium Ferrite ($La_xSr_{1-x}FeO_{3-\delta}$)
LSCF	Lanthanum Strontium Cobalt Iron Oxide ($La_xSr_{1-x}Fe_{1-y}Co_yO_{3-\delta}$)
L2SF55T	Lanthanum Strontium Iron Titanium Oxide ($La_{0.2}Sr_{0.8}Fe_{0.55}Ti_{0.45}O_{3-\delta}$)